04,06,13,14

DFT studies of nonlinear optical,piezoelectric, and photoelastic properties of hexagonal $M_2(NO_3)(OH)_3$ (M = Sr, Ba)

© Yu.N. Zhuravlev, E.V. Gvozdikova

Kemerovo State University,
Kemerovo, Russia

E-mail: zhur@kemsu.ru

Received April 9, 2025
Revised July 14, 2025
Accepted July 16, 2025

Within the framework of density functional theory, the structural, electronic, vibrational, dielectric, elastic, and piezoleastic properties of hexagonal $Sr_2(NO_3)(OH)_3$, $Ba_2(NO_3)(OH)_3$ are calculated using the coupled perturbed Hartree-Fock/Kohn-Sham method in a localized orbital basis set, employing the gradient-corrected PBE functional with D3(BJ) dispersion correction and the hybrid PBE0 and B3LYP functionals. Correlations between microscopic structural and macroscopic nonlinear optical, mechanical, and electromechanical characteristics are established based on the data obtained from the first principles.

Keywords: density functional, NLO crystals, dielectric constant, SGH coefficients, elastic constants, piezoelectric constants, nitrate hydroxides.

DOI: 10.61011/PSS.2025.07.61869.74-25

1. Introduction

Ultraviolet (UV) and deep ultraviolet (DUV) lasers have a very high single photon energy, which leads to their widespread use in semiconductor photolithography, medical and scientific instrumentation, and optoelectronic devices. However, it is not always possible to extract the wavelengths needed for these applications from a laser source itself. Therefore, the second harmonic generation (SGH) from nonlinear optical (NLO) materials is an important alternative method for obtaining them [1]. Currently, obtaining new UV-NLO materials with a good SHG characteristics and a short phase-matching cutoff wavelength is an important and challenging task [2].

From the point of view of their crystal structure [3], the NLO materials used and planned for use should have noncentrosymmetric (NCS) spatial symmetry groups, contain anions in π-delocalized systems, and active cations with lone pairs of electrons. In terms of their optical properties, they require [4] a short absorption edge or a large band gap, large SGH coefficients (g_{ij}) that should be higher than those of the standard sample KH_2PO_4 (KDP, ~ 0.39 pm/V [5]), moderate birefringence ($\Delta n = 0.07 \div 0.1$), as it is necessary for achieving phase-matching, and low dispersion of refractive indices. In addition, NLO materials must be chemically and mechanically stable, and large single crystals can be easily grown.

Over the past three decades, significant progress has been made in the field of DUV NLO materials, both in experimental studies and in theoretical design. A deep understanding of the „structure-property“ correlations makes it possible to strictly and accurately identify such crystals [3,6]. Extensive data has been accumulated in the literature, both on the general issues of new NLO materials [1,7–10] and their individual representatives — nitrates [2,11].

Metal nitrates can be obtained by relatively simple and energy-saving synthetic methods. However, they are easily soluble in water and therefore their studies as UV or DUV NLO materials are relatively scarce. Crystal structures consist of planar triangular structures NO_3^- with π-conjugated molecular orbitals. It is shown in Ref. [2] that many nitrate materials have higher SHG $4-5\,x$KDP responses than other types. Non-centrosymmetric nitrate $Sr_2NO_3(OH)_3$ was obtained by hydrothermal method in Ref. [12]. Due to the special coordination, the neighboring groups of NO_3 are perfectly parallel in the plane, which gives the maximum contribution to the nonlinear optical effect. The Kurtz-Perry method was used to show that the SHG coefficient in the powder sample is 3.6 times higher than in the KDP. The result of the diffuse reflection spectroscopy study showed that the short-wavelength absorption edge was below 200 nm, which makes it a promising NLO material for DUV radiation. Nitrate $Ba_2NO_3(OH)_3$ was synthesized in Ref. [13], and it demonstrates an ideal balance of high SHG coefficient, suitable birefringence, short UV absorption boundary, and physicochemical stability. The crystal structure of these compounds was previously studied in Ref. [14].

A new strontium nitrate hydrate $SrNO_3(OH) \cdot H_2O$ was synthesized in Ref. [15] by hydrothermal method, in which isolated anionic groups NO_3 are combined through polyhedra SrO_9 and form a three-dimensional network. Its diffuse reflectance spectra indicate that it has a UV cutoff edge of 288 nm. In another compound, $Sr(NO_3)_2 \cdot 4H_2O$ [16], nitrate groups form isolated one-dimensional chains. Strontium nitrate [17] also exhibits nonlinear properties, for

which various studies have been conducted, including X-ray diffraction, infrared, Raman, optical spectroscopy in the visible region and various mechanical measurements.

These non-centrosymmetric compounds are of great interest for materials science and engineering, since, in addition to NLO, they possess a number of other important physical properties and most of them have great potential applications in pyroelectricity, piezoelectricity, ferroelectricity [18]. For example, piezoelectrics — materials capable of converting stress into mechanical deformation or vice versa are an integral part of many medical applications and energy harvesting devices [19]. When a crystal is deformed, its optical properties change and this is described by photoelastic, piezo-optical tensors of the fourth rank, which correlate with changes in the dielectric constant tensor [20].

Basic methods currently play an important role in the description and prediction of the physical properties of crystals [21]. Therefore, in this work, within the framework of the coupled perturbed Hartree-Fock/Kohn-Sham (CPHF/KS) method, the structural, electronic, elastic, dielectric, piezoelectric, piezo-optic, photoelastic, and nonlinear optical properties of hexagonal strontium and barium nitrate hydroxides are calculated from first principles. This will enable a prediction of their potential applications as multifunctional materials.

2. Calculation method

The structure and physical properties of crystals were studied using density functional theory (DFT) and Hartree-Fock (HF) methods in the CRYSTAL17 software package [22]. Crystal orbitals are defined by linear combinations of localized atomic functions of Gaussian type, whose exponents and coefficients are determined from full-electron [23] and pseudopotential sets [24,25]. The exchange-correlation PBE [26] was used as DFT functionals, supplemented by an empirical variance correction in the form of D3(BJ) [27], as well as hybrid three-parameter B3LYP, which combines a 20 % Hartree-Fock exchange with an exchange B3 [28] and the correlation functional LYP [29] and PBE0 [30], in which there are no fitting parameters. The use of these functionals is due to the fact that due to the lack of experimental data on most of the studied characteristics, the theoretical forecast should include a reliable range of their values.

The thresholds controlling the accuracy of the Coulomb and exchange series are set equal 8, 8, 8, 8, 16 [31]. The inverse space is discretized using a grid 12×12 [32] with 133 independent $\boldsymbol{k}$ points in the irreducible part of the Brillouin zone. The accuracy of the self-matching procedure was no less than 10^{-10} a.u. (1 a.u. = 27.21 eV).

3. Crystal structure and chemical bond

Nitrate hydroxides $Sr_2NO_3(OH)_3$ (hereinafter — SNOH), $Ba_2NO_3(OH)_3$ (hereinafter BNOH) have a hexagonal lattice

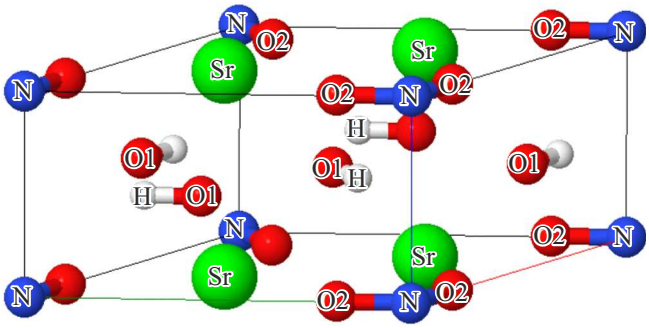

Figure 1. Unit cell $Sr_2(NO_3)(OH)_3$.

with the space group of symmetry $P\bar{6}2m$. The unit cell contains one formula unit with one unequal metal atom Sr, Ba (Wyckoff position 2c), nitrogen N (1a), hydrogen H (3g) and two oxygen atoms O1 (3g), O2 (3f). Each metal atom has in its environment 6 oxygen atoms O1 from the hydroxyl group OH and three oxygen atoms O2 from the nitrate NO_3. Its further environment consists of 6 hydrogen atoms and two metals. Each nitrate group is surrounded by six hydroxyl groups. The hydrogen atoms, in addition to the nearest O1, are surrounded by four O2 atoms. The crystallographic parameters calculated with various functionals, together with the available experimental data, are recorded in Table 1. The SNOH unit cell is shown in Figure 1.

The calculated lattice constants and interatomic distances correspond satisfactorily with the experimental ones. The standard deviations Δ calculated for 12 parameters indicate higher accuracy with the PBE0 functionality. However, it also has the lowest time performance. The fastest PBE functionality allows calculating deviations based on the lattice constants 2.4 %, for distances M-O 1.8 % and the worst for O-H at 15.1 %. Enabling the Van der Waals interaction (vdW) in the form of the PBE-D3 functionality significantly improves the constant (0.69 %), M-O distances (1.37 %) and degrades H-O (15.2 %). The dispersion energy is only -1.44 eV in SNOH and -1.36 eV in BNOH. Compromise values of Δ are achieved with the PBE0 functionality, which, unlike PBE, additionally includes Hartree-Fock exchange: 1.15, 1.33, 14.2 %.

Let us consider the microscopic parameters of the crystal structure and chemical bond, which can then be used in analyzing the macroscopic properties of crystalline systems. To do this, we will use the deformation density obtained by subtracting the densities of individual non-interacting atoms from the crystal density for a qualitative assessment, and the population density of overlapping electron shells of atoms calculated according to the Mulliken scheme $P_{A\text{-}B}$ for a quantitative assessment.

Figure 2 shows the distribution of the SNOH deformation density in the plane where $[SrNO_3]_\infty$ $(xy,\ z = 0)$ and in the plane $[OH]_\infty$ $(xy,\ z = 1/2c)$. The coordinate system is chosen so that the axis z is directed along the axis c.

Table 1. Calculated with the functionals PBE,PBE-D3, PBE0, B3LYP and experimentally measured (Exp [Ref]) crystal structure parameters $M_2(NO_3)(OH)_3$ ($M = Sr, Ba$): a, c — lattice constants, $M-O$ distances between metal and oxygen atoms, H−O — hydrogen and oxygen, N−O — nitrogen and oxygen. All values are specified in Å. Δ is the standard deviation (%) of theoretical and experimental data

Method	a, Å	c, Å	M-O1	M-O2	H-O1	H-O2	N-O2	Δ
$Sr_2NO_3(OH)_3$								
PBE	6.6780	3.6178	2.6572	2.8249	0.9804	2.5690	1.2741	5.98
PBE-D3	6.6146	3.5838	2.6338	2.7902	0.9799	2.5314	1.2728	6.10
PBE0	6.6192	3.5828	2.6344	2.8072	0.9698	2.5366	1.2531	5.48
B3LYP	6.6781	3.6154	2.6577	2.8328	0.9713	2.5656	1.2634	5.67
Exp [12]	6.6037	3.5585	2.6259	2.798	0.8193	2.5958	1.254	
$Ba_2NO_3(OH)_3$								
PBE	7.0098	3.8328	2.8078	3.0102	0.9856	2.6952	1.2764	6.49
PBE-D3	6.9443	3.8017	2.7862	2.9740	0.9851	2.6542	1.2753	6.44
PBE0	6.9622	3.8102	2.7907	2.9990	0.9745	2.6764	1.2553	5.97
B3LYP	7.0298	3.8535	2.8201	3.0293	0.9764	2.7085	1.2658	6.26
Exp [13]	6.9069	3.8028	2.7779	2.9785	0.8123	2.7468	1.241	

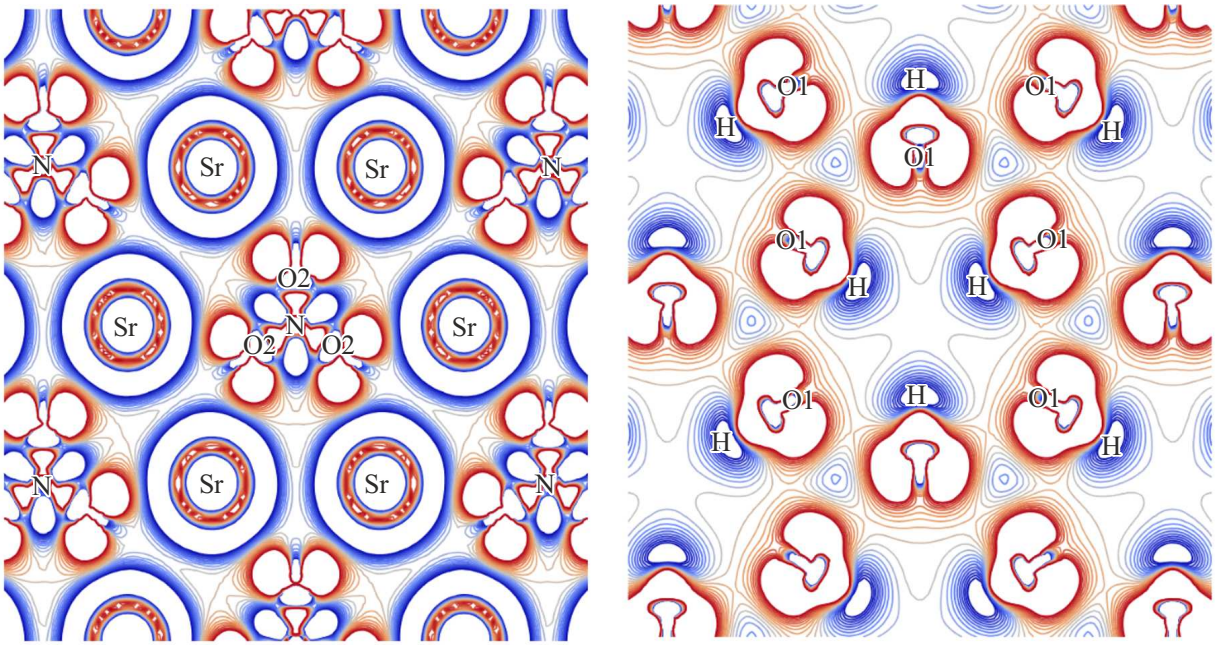

Figure 2. Distribution of deformation density in the plane xy $(z = 0)$ (left) and in the plane xy $(z = 1/2c)$ (right) in $Sr_2(NO_3)(OH)_3$.

Bond lengths, charge values, and overlap population density are important parameters of a chemical bond. The nitrate group NO_3 in the crystal lattice retains its geometry with the angle $\angle O_2\text{-N-}O_2$ in 120°, the bond length N-O2 1.2728 Å and the overlap population density $P_{N\text{-}O2} = 0.458\,e$, with a total charge of $-0.80\,|e|$ (here and below, calculation data with the PBE-D3 functionality are provided by default). All anions have a parallel orientation due to the interaction with strontium atoms. The angle ∠Sr-N-Sr is 120°, and the distance Sr-N is 3.8189 Å. Each strontium atom is surrounded by six oxygen atoms O1 at a distance of 2.6338 Å, the angle between which ∠O1-Sr-O1 is 85.7°, and the population density $P_{Sr\text{-}O1} = 0.007\,e$. For three O2 atoms, the Sr-O2 distances are greater — 2.7902 Å, the angle is $\angle O2\text{-Sr-}O_2$ 120°, and the population density is less. The charge flows from the region of the H atom in the $[OH]_\infty$ plane and flows into the O1 region, so that ions with charges $+0.13\,|e|$ and $-1.09\,|e|$ are formed, respectively. The total charge of atoms in this plane is thus negative, whereas in the $z = 0$ plane, due to the charge of the Sr ion in $+1.84\,|e|$, it is positive. The parameters of the chemical bond of the studied crystals are given in Table 2.

Table 2. Parameters of the chemical bond of nitrate hydroxides: E_g is the band gap (eV), Q_M, Q_H, Q_{HO}, Q_{NO_3} is the charges of metal atoms M =Sr, Ba, hydrogen H, anionic group OH, NO_3 (all in $|e|$), $P_{N\text{-}O2}$, $P_{H\text{-}O1}$ population density of overlap between atoms (units e — electron charge)

Crystal	Method	E_g	Q_M	Q_H	Q_{HO}	Q_{NO_3}	$P_{N\text{-}O2}$	$P_{H\text{-}O1}$
$Sr_2NO_3(OH)_3$	PBE-D3	2.36	1.84	0.13	−0.96	−0.80	0.458	0.442
	PBE0	5.21	1.87	0.20	−0.97	−0.84	0.468	0.431
	B3LYP	4.55	1.86	0.15	−0.96	−0.83	0.474	0.455
$Ba_2NO_3(OH)_3$	PBE-D3	2.41	1.48	0.24	−0.75	−0.71	0.489	0.417
	PBE0	5.18	1.55	0.30	−0.78	−0.76	0.503	0.409
	B3LYP	4.59	1.56	0.25	−0.79	−0.76	0.509	0.435

Thus, strontium and barium nitrate hydroxides have a layered structure, when two strontium atoms and a nitro group are located in one positively charged plane, and hydroxyl groups in a negatively charged plane. The coupling between the layers is electrostatic, as evidenced by the very high interaction energy of the sublattices −31.8, −25.5 eV, which is calculated as the difference between the total energy and the sum of the energy of the individual [$SrNO_3$], [OH]. The layered structure leads to anisotropy of elastic and piezoelectric properties.

Since the chemical bond in SNOH, BNOH is predominantly ionic, the energy distribution of electrons is characterized by relatively narrow bands in the valence band of the energy spectrum $E_n(\boldsymbol{k})$ and narrow bands in the spectrum of the density of states — Figure 3. The following designations of the points of the Brillouin zone k are used here in terms of the basic vectors of the inverse lattice: Γ (0,0,0), M (1/2,0,0), L (1/2,0,1/2), A (0,0,1/2), K (1/3,1/3,0), H (1/3,1/3,1/2). The beginning of the energy scale is aligned with the last filled state at the point Γ for SNOH and A in BNOH. The contributions of individual metal atoms, nitrate NO_3, and hydroxyl group in the partial density of states are highlighted in color.

The characteristics of the upper valence and lower conduction bands are important for describing the nonlinear optical properties and the cut-off threshold λ_{abs}. Three groups of bands with widths of 1.92, 1.0, 1.0 eV and maxima in the density of states at −0.3, −2.2, −4.1 eV are distinguished in the upper valence region of SNOH. The two upper valence bands are formed by p_{xy}-states of oxygen atoms from hydroxyl groups, and the next lower p-states of the nitro group. In the lower region of unoccupied states, there is a separate weakly dispersed zone with a width of 0.55 eV, crystalline orbitals, which are constructed from p_z-atomic orbitals of oxygen and nitrogen NO_3 groups. The minimum energy gap between the points Γ and A in SNOH is 2.36 eV. Only the next transition with an energy of 5.13 eV at the point Γ will be in s-state of metallic nature. In BNOH, the minimum transition takes place at the point A of the Brillouin zone and the width of the anionic band gap is 2.41 eV, and the anion band gap is 4.95 eV.

Thus, the chemical bond in nitrate hydrates is due to the strong ionic interaction of metal cations and anions of hydroxyl and nitrate groups, whose charges are greater for strontium compounds. The covalent bond within the anions will have a higher population density in NO_3 for the barium compound and a lower population in OH for strontium. Interionic electronic transitions are characteristic of the lower part and anion-cationic transitions for the upper part of the spectrum of electronic excitations. This structure of the energy zones of nitrate hydrates is manifested in nonlinear optical properties.

4. Crystal structure under pressure

When developing new NLO materials, it is necessary to study their behavior under pressure as a factor of stability under external influences. For this purpose, the dependences of the lattice constants $a(V)$, $c(V)$ and the total energy $E_{tot}(V)$ in the range of changes V/V_0 from 0.95 to 1.04 with a uniform step were calculated. A complete optimization of the structural parameters was conducted at each step. The dependence $E_{tot}(V)$ is approximated by the equation of state (EOS) in the Birch-Murnaghan form of the third order [33]

$$E(V) = E_0 + \frac{9V_0B_0}{16}\Big((x^{-2}-1)^3B_1 + (x^{-2}-1)^2(6-4x^{-2})\Big), \quad x = (V/V_0)^{1/3}$$

and its parameters are defined: E_0 is the total energy, V_0 is the equilibrium volume, $B_0 = -V(\partial P/\partial V)_T$ is the isothermal modulus of volumetric compression and $B_1 = (\partial B/\partial P)_T$ its first pressure derivative at $x = 1$. The dependence of pressure on volume is calculated using these parameters

$$P(V) = \frac{3B_0}{2}\left(x^{-7}-x^{-5}\right)\left(1+\frac{3}{4}(B_1-4)(x^{-2}-1)\right).$$

The EOS parameters are shown in Table 3.

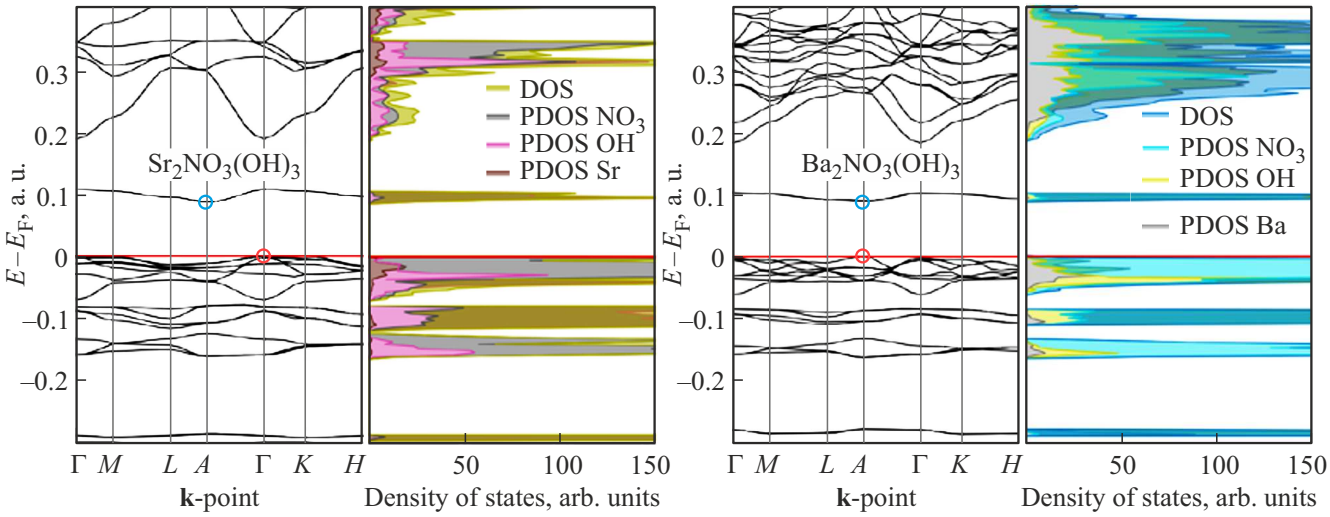

Figure 3. Band structure $E_n(\boldsymbol{k})$, total (DOS) and partial density of electronic states (PDOS) in $Sr_2NO_3(OH)_3$ (left) and $Ba_2(NO_3)(OH)_3$ (right).

Table 3. Parameters of the Birch-Murnaghan equation of state of the third order: E_0 — total energy (a.u.), V_0 — unit cell volume (Å^3), B_0 — volumetric module compression ratio (GPa), B_1 — its pressure derivative P.

Crystal	Method	$-E_0$	V_0	B_0	B_1
$Sr_2NO_3(OH)_3$	PBE	568.4658	139.708	58.41	4.58
	PBE-D3	568.5180	135.758	62.83	4.59
	PBE0	568.4375	135.950	62.13	4.71
$Ba_2NO_3(OH)_3$	PBE	558.1497	163.131	51.18	4.22
	PBE-D3	558.1990	158.785	54.23	4.23
	PBE0	558.0844	160.010	53.27	4.36

The quadratic decomposition was used to numerically represent the pressure dependences of constant lattices $a(P)$ and $c(P)$. The first and second derivatives for a in units of 10^{-3} are equal for SNOH: -35 Å/GPa, 1.3 Å/GPa^2, for BNOH: -43 Å/GPa, 1.8 Å/GPa^2. For the axis c, these will be -20 Å/GPa, 0.56 Å/GPa^2 and -23 Å/GPa, 0.63 Å/GPa^2, respectively. The speed of decreasing distances along the axis a is greater than along the axis c. This is due to the fact that ions of the same charge sign alternate along the axis c, and ions of the opposite sign alternate along the axis a (Figure 1). There is an almost linear relationship when the first coefficient is much greater than the second. This means that the linear module $B_{\text{A-O}} = -R_{\text{A-O},0}/(dR_{\text{A-O}}/dP)$ can be used to characterize changes in pressure between atomic distances $R_{\text{A-O}}$. The N-O bond is practically incompressible in SNOH, since the corresponding modulus is 1714 GPa (1648 GPa in BNOH). The module $B_{\text{H-O}}$ has an even greater value ~ 2600 GPa. On the contrary, the Sr-O1 and Sr-O2 bonds are characterized by much greater compressibility and the corresponding modules are 197 (181) and 145 (124) GPa. The distances between the centers of gravity of the cation and the anions in SNOH are characterized by the modules 287 GPa(Sr-H) and 189 GPa (Sr-N). The compressibility of the distances between the anions N-H is the largest and the corresponding modulus is 113 GPa.

Thus, under pressure, the greatest compressibility occurs for the distances between the centers of gravity NO_3 and OH, Sr, Ba, and anion cations, whereas the bonds N-O and H-O are practically incompressible. This means that intermolecular voids decrease in volume faster, and the molecules themselves practically do not deform.

5. Vibrational spectra

The vibrational spectra of Raman scattering and infrared absorption have important information for describing the properties of NLO materials. The frequencies ν_n are obtained by diagonalizing the mass-weighted Hesse matrix, which is determined by numerically differentiating the analytical gradients by the Cartesian coordinates of the atoms: $W_{\alpha_i,\beta_j}(\Gamma) = \frac{H_{\alpha i\beta_j}}{\sqrt{M_\alpha M_\beta}}$. Here $H_{\alpha i,\beta j}$ is the second derivative of energy, which is calculated numerically from analytical gradients, M_α and M_β are atomic masses; Greek and Latin indexes respectively refer to atoms and Cartesian coordinates. Details of the calculation of oscillatory frequencies can be found in Refs. [34,35].

Three regions are distinguished in the Raman and infrared absorption spectra of nitrate hydroxides. The low-frequency region with wavenumbers in the range $0 \div 400$ cm^{-1} is caused by lattice vibrations involving cations above 600 cm^{-1} intramolecular vibrations of nitrate ions are observed and above 3000 cm^{-1} — hydroxyl groups. The lattice region is unique for each compound, whereas the intramolecular ones have a similar appearance.

Table 4. Zero-point energy E_{v0} (kJ/mol) and wave numbers of intramolecular modes ν_4, ν_2, ν_1, ν_3 for NO_3 and ν_{OH} for OH (all cm^{-1}) calculated with PBE-D3, PBE0, and B3LYP functionals for strontium and barium nitrate hydroxides

Crystal	Method	E_{v0}	ν_4	ν_2	ν_1	ν_3	ν_{OH}
$Sr_2NO_3(OH)_3$	PBE-D3	145.92	613, 706	736, 977	1079	1451	3716, 3722
	PBE0	152.30	649, 726	806, 970	1079	1452	3867, 3877
	B3LYP	149.98	655, 726	820, 927	1116	1501	3825, 3831
$Br_2NO_3(OH)_3$	PBE-D3	138.22	637, 689	777	1059	1403	3667, 36677
	PBE0	149.75	697, 729	843	1147	1534	3802, 3804
	B3LYP	142.92	671, 710	850	1095	1455	3770, 3772

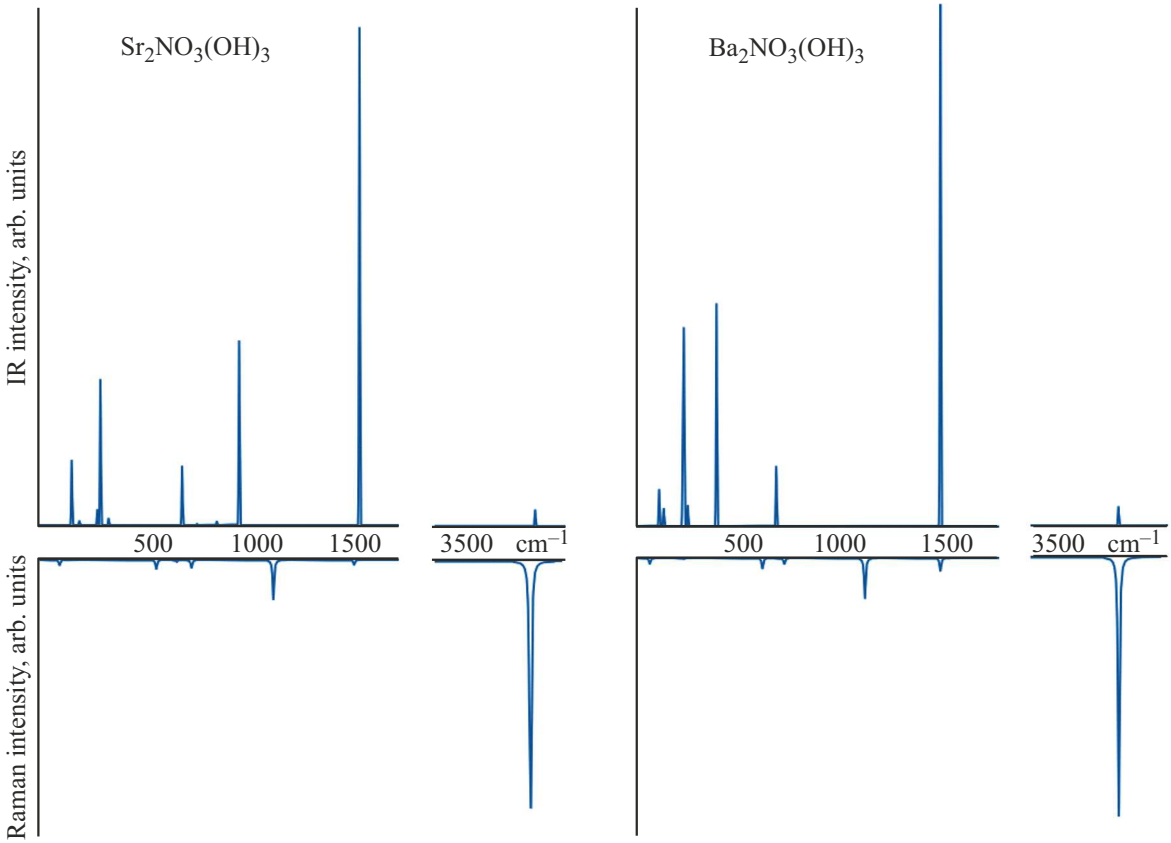

Figure 4. Infrared absorption (IR) and Raman scattering (Raman) spectra $Sr_2NO_3(OH)_3$ and $Ba_2NO_3(OH)_3$.

There are four types of vibrations for intramolecular vibrations NO_3: ν_4 is the planar deformation of the anion, ν_2 is out-of-plane deformation, ν_1 is the symmetrical stretching along the bond line N-O, ν_3 is the antisymmetric deformation in the plane. In addition to these modes, translational shifts of the anions as a whole and their rotations around the z axis will be observed in crystals.

The distribution of vibrational modes over irreducible representations looks as follows in SNOH, BNOH: $\Gamma_{vib} = 3A_1'(\mathrm{RS}) + 3A_2' + A_1'' + 4A_2''(\mathrm{IRS}) + 8E' + 3E''(\mathrm{RS})$. The number in front of the symbol of the irreducible doubly degenerate representation E and the single one A indicates the number of oscillations, and the type of activity in parentheses: IRS is the infrared absorption spectra, RS is the Raman light scattering. There is a negative mode for nitrate hydroxides, which indicates their dynamic instability. IRS and RS are shown in Figure 4, and the wave numbers of intramolecular oscillations in Table 4

The energy of zero vibrations $E_{v0} = \Sigma_i^N h\nu_i/2$, where summation is carried out over the total number of vibrations N, equal to the number of atoms in a unit cell multiplied by 3, will take maximum values for the PBE0 functional. A satisfactory coincidence of the calculated frequencies with the experimental data [13,14] is observed

for the B3LYP functional. Therefore, in the future, its values will be used to quantify the vibrational modes.

In the IR spectrum of SNOH, the most intense mode (1628 km/mol, 100 %) is the ν_3 mode of E' symmetry with a wavenumber of 1501 cm^{-1}, and the ν_2 mode of symmetry A''_2 (37 %) with a wavenumber of 927 cm^{-1}. For BNOH, these are the modes at 1455 (1980 km/mol, 100 %), 386 (37 %) and 230 (31 %) cm^{-1}. The latter are formed by z-translational vibrations of barium atoms and a nitro group, as well as xy-vibrations of barium and a hydroxyl group. The mode $\nu_2 = 820\,cm^{-1}$ has an incomparably lower intensity. The ν_4 modes of E' symmetry at 726.655 cm^{-1} form two other bands of different intensity in SNOH. Lattice vibrations with an intensity of 16, 13 % at 265, 128 cm^{-1} belong to xy-translational vibrations of strontium and nitrate, hydroxyl groups.

Three optical oscillations of symmetry E' and A'_1 are distinguished in the Raman spectrum. The full-symmetric A'_1 vibration with wavenumber in SNOH 3831 cm^{-1} (in BNOH 3772 cm^{-1}) is the most intense (assumed to be 100 %). The mode of E' symmetry is next to it at 3825 cm^{-1} (3770) with intensity 67 % (33 %). The first is formed by z-, and the second by xy-displacements of hydrogen and oxygen atoms O1. It is the overwhelming intensity of these fluctuations that explains the scarcity of the RS spectrum (Figure 4). The band ν_1 has a noticeable intensity at 1116 (1095) cm^{-1} and the band ν_4 has a noticeable intensity at 726 (710) cm^{-1}. Rotational mode of symmetry E'' with wavenumber 557 (605) cm^{-1} and intensity of 5 % is barely noticeable.

Thus, the vibrational spectra of nitrate hydrates reflect the anionic dominance in the frequency spectrum above 600 cm^{-1}, the different atomic mass of cations in the lattice, and their polarization dependence — the layered structure of crystals.

6. Elastic and mechanical properties

Crystalline NLO materials must have mechanical stability, hardness, lack of spreading, ease of processing, etc. Therefore, when designing them, it is necessary to investigate elastic properties as a factor of static mechanical stability.

The components of the elasticity matrix C_{ij} in Voigt notation $i, j \to \{1 — xx, 2 — yy, 3 — zz, 4 — yz, 5 — xz, 6 — xy$ has dimension 6×6 and is defined in terms of the second derivative of the total energy with respect to deformations $C_{ij} = \frac{1}{V}\frac{\partial^2 E_{tot}}{\partial\eta_i \partial\eta_j}$. The CRYSTAL software package can calculate elastic tensors using the automated procedure described in Refs. [36,37]. The accompanying formulas are given in Ref. [38].

There are no experimental measurements of elastic constants and modules for the studied crystals. Therefore, for comparative characteristics, we will focus on the KDP measured for crystals, which are widely used in laser ignition installations as components of optical switching and frequency conversion. These crystals are soft, brittle and sensitive to external conditions [39]. There are also calculations of the elastic properties of $Sr(NO_3)_2$, $Ba(NO_3)_2$ in symmetry $Pa\bar{3}$ [40] performed by the CRYSTAL package with PBE functionality, as well as their experimental values. The calculated unique elastic constants are shown in Table 5. The constant $C_{66} = (C_{11} - C_{12})/2$.

There are relations between the elastic constants that follow from the need to fulfill the criterion of stability of the crystal lattice [42]. Necessary and sufficient conditions for elastic stability are written for all types of symmetries in Ref. [43]. They have the following form in a hexagonal crystal: $C_{44} > 0$, $C_{11} > |C_{12}|$, $(C_{11} + C_{12})C_{33} > 2C_{13}^2$. Another condition $C_{33} > C_{13}$ is obtained in Ref. [44] from the conservation law. Elastic constants for SNOH and BNOH crystals satisfy the requirements of mechanical stability for all functionals.

The elastic properties of a hexagonal crystal in the plane of the layer (xy) are isotropic and are described by the constants C_{11} and C_{12}, which characterize the Young's modulus and Poisson's ratio. The constant C_{33} determines the Young's modulus, and the constant C_{13} determines the Poisson's ratio in the perpendicular (z) direction. The elastic constant C_{11}, which reflects the measure of stiffness against unidirectional deformation along the axis a, is less than the constant C_{33}, which allows evaluating the elastic response of the material to unidirectional stress along the axis c. The constant C_{44} describes the stresses when the layers are shifted relative to each other. It can be seen from Table 5 that SNOH will have the greatest resistance to compression/stretching along the axis of a, while BNOH will have the least. The shear constants C_{44} are less than the compression/stretching constants, which means that the layers $[M_2AO_3]_\infty$ and $[OH]_\infty$ can move relatively freely relative to each other.

Table 6 shows the volumetric module of a single crystal calculated with various functionals B_R (characterizes the ability to change volume under the influence of a comprehensive voltage, the same in all directions) and linear modules B_a and B_c (characterize the ability of a crystal to change its volume under the influence of voltage along the axes a and c). The module B_R agrees well with the data in Table 3, and it differs little for different functions. The elastic anisotropy of crystals is important because it is closely related to the possibility of microcracks in single crystals. The shear coefficient is used to quantify the elastic anisotropy of single crystals [45]: $A = 4C_{44}/(C_{11} + C_{33} - 2C_{13})$. For an isotropic crystal $A = 1$, and the amount of deviation in one direction or the other is a measure of elastic anisotropy. This parameter is equal to 0.55 in SNOH, 0.52 in BNOH, and 0.51 in KDP. Taking into account vdW in the PBE-D3 functionality leads to the fact that both crystals have the largest modules for it, which means their high resistance to deformation and, consequently, lower compressibility.

The elastic constants calculated with different functionals have similar values, they are larger for SNOH than for BNOH. The constants of tension/compression exceed the

Table 5. Elastic constants C_{ij} (GPa) and density ρ of single crystals of nitrate hydroxides calculated with the functionals PBE, PBE-D3, PBE0 and experimental values for DP

Crystal	Method	ρ, g/cm^3	C_{11}	C_{12}	C_{33}	C_{13}	C_{44}
$Sr_2NO_3(OH)_3$	PBE	3.432	98.7	48.8	119.1	29.4	22.0
	PBE-D3	3.532	108.3	50.9	123.1	31.1	23.2
	PBE0	3.528	105.3	50.9	125.0	30.2	24.9
$Ba_2NO_3(OH)_3$	PBE	3.958	79.4	43.3	98.4	30.0	16.4
	PBE-D3	4.066	85.2	45.0	101.6	31.9	16.0
	PBE0	4.037	82.4	45.0	103.1	30.9	18.1
KDP	Exp. [41]		71.2	−5.0	56.8	14.1	12.6

Table 6. Volumetric modulus of elasticity B_R, linear Young's modules E_a, E_c, linear modules B_a, B_c along the axes a, c (all in GPa) single crystals of nitrate hydroxides

Crystal	Mehtod	B_R	B_a	B_c	E_a	E_c
$Sr_2NO_3(OH)_3$	PBE	59.1	176.6	178.5	72.6	107.4
	PBE-D3	62.8	191.9	182.0	82.1	111.0
	PBE0	62.0	186.8	184.7	78.6	113.3
$Ba_2NO_3(OH)_3$	PBE	51.5	150.2	164.0	53.6	83.7
	PBE-D3	54.4	160.6	168.6	59.0	85.9
	PBE0	53.3	155.5	171.3	55.7	88.1
KDP	Exp. [41]	27.3	78.8	88.5	66.6	50.8

shear constants, and the linear Young's modules along the c axis are significantly larger than for the axis c. Thus, the elastic properties of single crystals reflect their layered structure.

Most materials are polycrystalline, consisting of aggregated crystallites. Their elastic properties were calculated using the Voigt (V)-Reus (R)-Hill (H) [46–48] model. Voigt and Reus established boundaries for the volume modulus B_V, B_R and the shear modulus G_V, G_R, which are determined from statistical models for describing elastic deformation of polycrystalline materials. Voigt assumed that the elasticity matrix $C_V = \langle C \rangle$ is averaged, and the compliance matrix $S_R = C_R^{-1}$, $S_R = \langle S \rangle$ is averaged by Reus. Voigt and Reus boundaries converge when the crystallites inside the aggregate are isotropic. Hill suggested using their average values $B_H = (B_V + B_R)/2$, $G_H = (G_V + G_R)/2$ as modules, which are in better agreement with the experiment. Moreover, the Young's modulus and Poisson's ratio can be obtained as $E_H = 9B_H G_H/(3B_H + G_H)$, $\mu = (3B_H - 2G_H)/(6B_H + 2G_H)$. The corresponding values are listed in Table 7.

The volumetric stiffness modulus of polycrystals B_H, as well as the shear modulus G_H, which characterizes the ability of a material to resist shape change while maintaining its volume, take the highest values in SNOH and lower values in BNOH. The values B_H, G_H do not exceed those in nitrates [40], where they are 32.2, 27.1 GPa for $Sr(NO_3)_2$ and 27.1, 9.1 GPa for $Ba(NO_3)_2$. The relatively small values of GH indicate that shear deformation occurs under a certain stress and it is this deformation that limits the stability of hexagonal NLO materials.

Brittle or ductile behavior is crucial for the possible application of NLO material. An experimental criterion is proposed in Ref. [49] for their difference in the form of the ratio of the volumetric compression modulus to the shear modulus: if it is greater than 1.75, the material will be plastic, otherwise it will be brittle. It follows from Table 7 that the ratio B_H/G_H is more than twice, and this indicates the plasticity of nitrate hydrates. It is known [50] that the Poisson's ratio of covalent materials is small ($\mu \sim 0.1$), while the typical value for ionic materials is 0.25. In addition, the Poisson's ratio also characterizes plasticity or brittleness. Its value is less than 1/3 typical for brittle materials and its greater value is typical for ductile materials [51]. The values of μ in Table 7 indicate the predominantly ionic nature of the chemical bond with a small amount of covalence, on the one hand, and plasticity, on the other hand.

Knowing the modules B_H, G_H, it is possible to calculate the velocities of elastic waves [52], and through it determine the Debye temperature [53]:

$$\theta_D = \frac{h}{k_B}\left(3\frac{N}{4\pi}N_A\frac{\rho}{M}\right)^{1/3} v_{cp},$$

where h is the Planck's constant, k_B is the Boltzmann's constant, N_A is the Avagadro's constant, N, M is the number of atoms in a formula unit and its molecular weight. The Debye temperature is a physical constant that characterizes many properties of crystals: heat capacity, electrical conductivity, thermal conductivity, melting point, etc. A higher Debye temperature implies a higher thermal conductivity. Under normal laser operating conditions, its working substance inevitably heats up, therefore, in order

Table 7. Elastic properties of polycrystalline nitrate hydroxides: B_H — volumetric modulus, G_H — shear modulus, E_H — Young's modulus (all in GPa), μ — Poisson ratio, Θ_D — Debye temperature (K), k_{min} — thermal conductivity coefficient (W/mK) calculated with the functionals PBE, PBE-D3, PBE0

Crystal	Method	B_H	G_H	E_H	μ	Θ_D	k_{min}
$Sr_2NO_3(OH)_3$	PBE	59.1	26.8	69.8	0.303	410	1.05
	PBE-D3	62.9	29.2	75.8	0.299	426	1.10
	PBE0	62.0	29.5	76.3	0.295	428	1.11
$Ba_2NO_3(OH)_3$	PBE	51.5	19.7	52.5	0.330	312	0.77
	PBE-D3	54.4	20.5	54.7	0.333	317	0.79
	PBE0	53.5	21.0	55.8	0.326	321	0.79

Table 8. Calculated with the PBE-D3, B3LYP functional wave numbers of lattice LO symmetry modes A_2'' and E' (LO-TO splitting, cm^{-1}) in nitrate hydrates

Crystal	Method	A_2''	E'
$Sr_2NO_3(OH)_3$	PBE-D3	240(0.5)	163(20), 185(11), 344(69), 302(−0.5)
	B3LYP	274(23)	155(27), 170(6), 344(78), 301(−3)
$Ba_2NO_3(OH)_3$	PBE-D3	251(34)	126(7), 156(11), 320(74), 243(1)
	B3LYP	268(43)	122(10), 143(9), 312(82), 246(−2)

to find out whether the material is a potential candidate for NLO, it is necessary to investigate its thermal conductivity. Using existing theories of minimum thermal conductivity a theoretical minimum has been developed in Ref. [54] that can be calculated after replacing various atoms with an equivalent atom with an average atomic mass:

$$k_{min} = k_B N_A^{2/3} N^{2/3} \rho^{-1/2} M^{-2/3}.$$

The calculated values of the Debye temperature and the coefficient of thermal conductivity are shown in Table 7. According to the data from Ref. [55], the experimental thermal conductivity for KDP is 1.21 for the parallel direction and $1.34\,m^{-1}K^{-1}$ for the perpendicular. In strontium and barium nitrates, according to the data from Ref. [40], the Debye temperature is 282, 243 K, respectively, and the thermal conductivity coefficient is 0.55, 0.45,$Wm^{-1}K^{-1}$. The experimental data for Θ_D in these compounds from thermodynamic data are 249, 196 K and 237, 218 K from X-ray diffraction [56].

Thus, polycrystalline hydrates of strontium and barium nitrates are plastic materials with a higher Debye temperature and thermal conductivity coefficient than the corresponding nitrates.

7. Dielectric properties

Long-range Coulomb effects are neglected in the case of ionic compounds due to the coherent displacement of the nuclei. Therefore, the Hesse matrix needs to be adjusted to obtain longitudinal optical (LO) modes [57]. This additional contribution, the so-called non-analytical term, depends on the dynamic permittivity tensor and the Born effective charge tensor. Knowing them, we can calculate the corresponding LO-TO splitting. The real and imaginary parts of the complex permittivity $\varepsilon_{ij}(\nu) = \varepsilon_{1,ij}(\nu) + i\varepsilon_{2,ij}(\nu)$ are calculated in the CRYSTAL program code for each unequal polarization direction based on the classical Drude-Lorentz model. The maxima $\varepsilon_2(\nu)$ and $\mathrm{Im}(-1/\varepsilon(\nu))$ (loss functions) correspond to TO and LO frequencies ν, respectively. The reflection coefficient curve is calculated for each unequal polarization direction using the formula

$$R_{ii}(\nu) = \left| \frac{\sqrt{\varepsilon_{ii}(\nu) - \sin^2\theta} - \cos\theta}{\sqrt{\varepsilon_{ii}(\nu) - \sin^2\theta} + \cos\theta} \right|^2,$$

where θ is the angle between the incident ray and the normal to the crystal surface [58].

The static permittivity tensor has electronic ε_{ij}^{el} and ionic ε_{ij}^{vib} components. The nuclear contributions to the dielectric constant are introduced by [20] summing over the phonon modes of the effective Born vectors [59], in which the dynamic charge tensor is determined by multiplying the first derivative of polarization by atomic displacements multiplied by the cell volume when the applied electric field is zero.

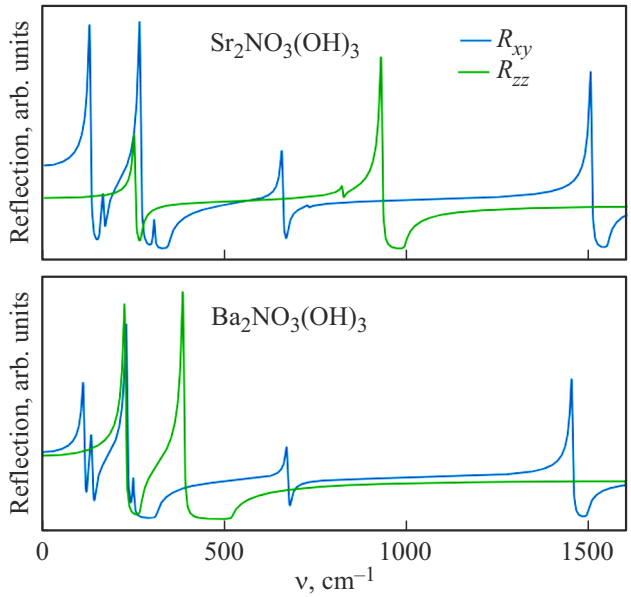

Figure 5. Reflection coefficient with plane polarization xy (R_{xy}) and in the direction of the axis z (R_{zz}) for $Sr_2NO_3(OH)_3$ (top) and $Ba_2NO_3(OH)_3$ (bottom).

The frequency dependences of the reflection coefficient are shown in Figure 5. $\varepsilon(\nu)$ is a diagonal tensor in hexagonal crystals, so only the components $xx = yy$ and zz are nonzero. The width of the bands is determined by LO-TO splitting, and the maxima and minima correspond to the frequencies of TO, LO modes. The main features of the spectra are caused by lattice vibrations and fluctuations inside nitrate ions. The spectral range above 3000 cm^{-1} and has a very low intensity and therefore it is absent in Figure 5. Vibrational symmetry modes A_1', E''LO-TO do not experience a shift. The wave numbers LO of lattice vibrational modes, together with the value of LO-O splitting (in parentheses) are given in Table 8.

The model of ionic compounds, in which studies of dielectric properties are performed, is sensitive to the choice of functional. Therefore, the calculations of the functions of the complex dielectric constant and reflection coefficient were carried out with PBE-D3 and B3LYP functionals. Further in the text, numerical information is provided for PBE-D3, and B3LYP values are given in parentheses for comparison.

SNOH has a low-intensity band in the reflection spectrum of OH^- in the region of 3715 cm^{-1} (3825 cm^{-1} for B3LYP), the width of which taking into account the LO-TO splitting $(\Delta\nu)$ for the E' symmetry mode is 0.7 (0.6) cm^{-1}. The low value of $\Delta\nu$ is attributable to the fact that this oscillation is formed by oppositely directed displacements relative to heavy oxygen atoms and light hydrogen atoms. The other atoms do not participate in it. There is also no noticeable splitting of ~ 1 cm^{-1} modes with maxima 732 (820), 703 (726) cm^{-1}, whereas modes 1449, 1078 (1501, 927) cm^{-1} have $\Delta\nu = 45$, 69 see^{-1} (47, 68 cm^{-1}). The large polarization (xx, zz) differences in the wavenumbers of the same type of vibrational modes are due to the anisotropy of the dynamic charge tensor of oxygen and hydrogen atoms.

Table 9. Electronic (el) and ionic (vib) components of the dielectric constant tensor ε calculated with the functionals PBE-D3 and B3LYP

Crystal	Method	ε_{xx}		ε_{zz}	
		el	vib	el	vib
$Sr_2NO_3(OH)_3$	PBE-D3	2.33	3.54	1.91	0.28
	PBE0	2.17	3.63	1.80	0.26
	B3LYP	2.13	3.94	1.78	0.52
$Ba_2NO_3(OH)_3$	PBE-D3	2.78	3.82	2.58	4.49
	B3LYP	2.51	4.14	2.32	3.84

Lattice vibrations also experience various LO-TO splits. Translational modes lead to large $(70-80\,\text{cm}^{-1})$ values of $\Delta\nu$ at 274 (265) cm^{-1}. Modes with a negative value are of particular interest when the wave number of the LO mode is less than that of the TO mode. Such is the oscillation E' of the symmetry at 301 (304) cm^{-1}, in which the atoms of the nitro group move synchronously in the plane xy, and the hydroxyl groups move asynchronously.

The values of the static permittivity tensor are given in Table 9. Electronic (el) and ionic components taking into account lattice vibrations (vib) are indicated here. They define the extreme points in Figure 5. As a rule, the relaxed components ε are more electronic for xx- and less for zz-, which reflects the contributions of the electronic and vibrational subsystems of the crystal. Heavy barium cations make a significant contribution to the lattice modes, which significantly enhances the zz-component in BNOH. The total dielectric constant is obtained by summing the contributions.

Thus, the dielectric properties of nitrate hydroxides are described using the frequency dependence of the dielectric constant and the reflection coefficient. Lattice vibrations up to 400 cm^{-1} with a pronounced polarization dependence have a significant intensity in them. The ionic contribution to the dielectric constant dominates for the xx-component in both compounds, whereas the zz-component dominates only for BNOH.

8. Piezoelectric properties

The mathematical description of piezoelectricity relates strain (or stress) to an electric field through a third-order tensor. In linear approximation, the direct **e** and inverse **d** piezoelectric tensors express polarization **P** induced by deformation $\boldsymbol{\eta}$ $P = e \times \eta|_{E=\text{const}}$ and deformation induced by an external electric field **E** $\eta = d^T \times E|_{\sigma=\text{const}}$,

Table 10. Direct e_{ij} (C/m^2) and inverse d_{ij} (pm/V) piezoelectric constants of strontium and barium nitrate hydroxides. Electronic (el) and nuclear (vib) contributions to constants are given

Crystal	Method	e_{22}		d_{22}		d_{16}	
		el	vib	el	vib	el	vib
$Sr_2NO_3(OH)_3$	PBE-D3	0.13	−0.29	2.24	−5.06	4.49	−10.13
	PBE0	0.13	−0.29	2.30	−5.31	4.59	−10.62
$Ba_2NO_3(OH)_3$	PBE-D3	−0.08	0.25	−1.99	6.30	−3.97	12.61
	PBE0	−0.09	0.27	−2.32	7.15	−4.65	14.26

Table 11. Independent photoelastic pij constants for nitrate hydroxides

Crystal	Method	p_{11}	p_{12}	p_{33}	p_{13}	p_{31}	p_{44}
$Sr_2NO_3(OH)_3$	PBE	0.369	0.248	0.151	0.191	0.298	−0.124
	PBE-D3	0.371	0.248	0.152	0.179	0.303	−0.146
	PBE0	0.295	0.221	0.198	0.222	0.260	−0.192
$Ba_2NO_3(OH)_3$	PBE	0.269	0.233	0.111	0.234	0.285	−0.049
	PBE-D3	0.269	0.234	0.114	0.227	0.285	−0.094
	PBE0	0.264	0.233	0.154	0.254	0.278	−0.065

respectively. Piezoelectric constants can be calculated in Voigt notation as $e_{ij} = \partial P_i/\partial \eta_j]_{\mathrm{E}} = \partial \sigma_j/\partial E_i]_{\eta}$, where **P**, **E**, η, σ represent the electric displacement field, electric field, strain tensor, stress tensor, respectively. Piezoelectric strain constants are often used in the literature, denoted as $d_{ki} = \partial P_k/\partial \sigma_i]_{\mathrm{E}} = -\partial \eta/\partial E_k]_{\sigma}$. They can easily be associated with constants e_{ij} through constant compliance matrices $d_{ik} = e_i l \times S_{lk}$. Piezoelectric constants can be decomposed into contributions of electronic „trapped ions“ and nuclear„internal deformations“ [60] $e_{ij} = e_{ij}^{clamp} + e_{ij}^{relax}$. The nuclear term measures the piezoelectric effect due to relaxation of the relative positions of atoms caused by deformation. The automated computational procedure is described in Refs. [61,62]. The direct constant in the standard piezoelectric material α-quartz e_{11} is 0.15 C/m^2 at room temperature and 0.07 C/m^2 at temperatures up to 5 K [63]. The inverse constant $d_{11} = 2.0 \sim 2.3$ pm/V [64].

Direct and inverse piezo constants for nitrate hydrates are listed in Table 10. The electronic and nuclear components are listed separately. The total piezoelectric constants are obtained by summation.

The value of the constant $e_{11} \equiv e_{xxx}$ measures the polarization induced along x by deformation η_{xx}. Its maximum value for the PBE0 functional is 0.13 C/m^2 is for SNOH and less than 0.09 C/m^2 is for BNOH. This piezoelectric response is somewhat less than that of α-quartz. The inverse constants are the result of the relationship between the direct piezoelectric constants and the compliance constants S_{ij}. The inverse piezoelectric constant $d_{11} = d_{22}$ is approximately the same for these compounds, and the constant d_{26} is greater in BNOH. The significant difference between the electronic and vibrational components of the piezoelectric constants is natural. For instance, it was found in a typical ferroelectric $SrTiO_3$ of symmetry $Ima2$, according to data from Ref. [60], that, for example, the electronic component of the constant e_{11} is 0.02 C/m^2, and the relaxed 9.28 C/m^2. The corresponding components are 0.02 and 33.51 pm/V for the inverse constant d_{11}. The sign does not play a role here, since the value of the constant modulus is determined in the experiment [65].

As follows from Table 10, the effects of nuclear relaxation play an important role, up to a sign change. Let's take this as an example of SNOH. Calculated in the CPHF/KS approximation with a PBE0 functional, the electronic piezoelectric tensor has a single nonzero component $e_{22} = 0.13$ C/m^2. Taking into account the vibrational structure of the crystal, the ionic component will be equal to -0.29 C/m^2. The largest contribution (-0.335 C/m^2) to its formation is made by the lattice symmetry mode E' with a wave number of 136 cm^{-1}, the intramolecular mode at 1565 cm^{-1} (-0.163 C/m^2). Modes with wave numbers 169 cm^{-1}, 272 cm^{-1} give a positive contribution of 0.101 C/m^2 and 0.109 C/m^2, respectively. The contribution of other fluctuations is less noticeable.

Thus, possessing a non-centrosymmetric lattice, nitrate hydrates exhibit piezoelectric properties, with values of direct constants no greater and inverse constants no less than those in α-quartz, which is typical among such materials.

Table 12. Independent piezo-optical π_{ij} (TPa^{-1}) constants for nitrate hydroxides

Crystal	Method	π_{11}	π_{12}	π_{33}	π_{13}	π_{31}	π_{44}
$Sr_2NO_3(OH)_3$	PBE	3.170	0.761	0.300	0.630	1.960	−5.648
	PBE-D3	2.906	0.778	0.303	0.523	1.844	−6.299
	PBE0	2.125	0.758	0.858	1.077	1.498	−7.707
$Ba_2NO_3(OH)_3$	PBE	2.229	1.216	−0.336	1.324	2.408	−2.962
	PBE-D3	2.074	1.193	−0.308	1.213	2.268	−5.911
	PBE0	2.007	1.157	0.218	1.517	2.127	−3.619

9. Photoelastic properties

The change in the components of the inverse permittivity tensor ε^{-1}, under the action of deformation, is determined by deformation-optical coefficients (i. e., elements of the fourth-rank elastic-optical or photoelastic Pockels tensor p): $\Delta\varepsilon_{ij}^{-1} = p_{ijkl} \times \eta_{kl}$. In Voigt's notation, the photoelasticity constants can be obtained as $p_{ij} = (\partial_i^{-1})/\partial\eta_j)$. The piezo-optical tensor of the fourth rank π, whose elements are the stress-optical coefficients π_{ij}, can be obtained from a photoelastic p and elastic as $\pi = p \times S$ or $p = \pi \times C$. Unlike the elasticity and compliance tensors, the tensors p and π are not symmetrical, so the number of components determined for optical stress and optical strain tensors is greater than for elasticity tensors. The photoelastic constants p_{ij} are dimensionless, whereas the piezo-optical constantsπ_{ij} are usually expressed in Brewster units: $1\,\mathrm{Br} = 10^{-12}\,\mathrm{Pa}^{-1} = 1\,\mathrm{TPa}^{-1}$.

An automated scheme has been developed in Refs. [20,66] for the theoretical calculation of the photoelastic and piezo-optical tensor of the fourth rank of crystals belonging to any spatial symmetry group, which requires simultaneous determination of tensors of elastic stiffness C, compliance S.

Table 11 shows the calculated independent components of the photoelasticity tensor of metal nitrate hydroxides.

Experimental data on photoelastic constants are not available, so the constants for α-quartz can be used for comparison [67]. Other well-known materials for which calculated and experimental data are available are $CaWO_4$ [68], as well as for ionic MgO, NaCl [20]. The photoelastic constants for $Sr(NO_3)_2$, $Ba(NO_3)_2$) were calculated earlier in Ref. [40]. So for $Sr(NO_3)_2$, the experimental (calculated) values of the constants are equal for $p_{11} = 0.18\,(0.20)$, $p_{12} = 0.36\,(0.38)$, $p_{44} = -0.00\,(-0.01)$.

The photoelastic constants in the plane xy assume the highest values. For the direction of z, the value of p_{33} is about three times less than in the plane, and it is slightly higher than the experimental and theoretical values in quartz. The shear coefficients are negative and their highest values are in SNOH crystals. The value of p_{44} in BNOH is comparable to quartz and significantly higher than in barium nitrate.

The piezo-optical coefficients π_{ij}, where $i,\ j = 1, 2, 3$, describe the relationship between the main refractive indices and the normal voltage (Table 12). They are called the main coefficients. The coefficients π_{ij}, where $i = 1,\ 2,\ 3$ and $j = 4,\ 5,\ 6$, relate the main refractive indices to tangential stresses and are called shear coefficients. The piezo-optical coefficients π_{ij}, where $i = 4,\ 5,\ 6,\ j = 1,\ 2,\ 3$ correspond to the rotation of the optical indicatrix and are called rotational. They are zero everywhere. The rotational-shear coefficients correspond to the indices $i = 4,\ 5,\ 6,\ j = 4,\ 5,\ 6$. All crystals have a single crystal, but it is not listed in the tables, as it is expressed in terms of π_{11} and π_{12}.

The calculated photoelastic and piezooptical coefficients indicate significant differences in the tensors of optical stresses and optical deformations in hydrates of strontium and barium nitrates.

10. Nonlinear optical coefficients

Polarizability α, first hyperpolarizability β, second hyperpolarizability γcan be analytically evaluated using the CPHF/KS [69,70] procedure. The corresponding tensors are related to the dielectric susceptibility of the first $\chi^{(1)} = 4\pi\alpha/V$, the second $\chi^{(2)} = 2\pi\beta/V$, and the third $\chi^{(3)} = 2\pi\gamma/3V$ orders, which are the coefficients of the linear relationship between the polarization of the dielectric and the external electric field: $P = \varepsilon_0(\chi^{(1)}E + \chi^{(2)}E^2 + \chi^{(3)}E^3 + \ldots$. The first order electrical susceptibility allows determining the refractive index tensor $\chi^{(1)} = n^2 - 1$, the second order electrical susceptibility allows determining the generation coefficient of the second harmonic $g = \chi^{(2)}/2\,(\mathrm{a.u.})$ and the third order electrical susceptibility allows determining the intensity of the Raman spectrum.

The requirements for nonlinear materials include, in particular, the presence of a large SHG coefficient and moderate birefringence. For uniaxial hexagonal systems, double refraction is the difference in the refractive indices of ordinary and extraordinary rays, i. e. $\Delta n = |n_o - n_e|$. Here, the index e corresponds to excitation by a polarized

Table 13. Second harmonic generation coefficient g (pm/V) and double refraction Δn, calculated with the functionals PBE-D3, PBE0, B3LYP

Crystal	g, Δn	PBE-D3	PBE0	B3LYP
$Sr_2NO_3(OH)_3$	g	2.172	0.696	0.769
	Δn	0.143	0.125	0.126
$Ba_2NO_3(OH)_3$	g	0.597	0.282	0.341
	Δn	0.062	0.060	0.061

electromagnetic wave, the electric field of which is parallel to the optical axis of the crystal (axis c), and the index o corresponds to excitation by a polarized electromagnetic wave, the electric field of which is perpendicular to c.

The coefficients of second harmonic generation g and double refraction Δn calculated using the functionals PBE-D3, PBE0 and B3LYP are shown in Table 13.

Experiments [12,13] show that SNOH and BNOH are phase-consistent and the SHG coefficients are 3.6 and 4 KDP units at a wavelength of 1064 nm. According to data from Ref. [2], the birefringence in BNOH is 0.082 at a wavelength of 532 nm and it is equal to 0.080 at 589.6 nm. The coefficients calculated in Table 13 are g higher for SNOH than in BNOH, which contradicts the experiment. On the contrary, the double refraction is smaller in BNOH, and it is close to the experimental one [13]. The theoretical results given here are indicated for the case of an infinite wavelength. The dependences of the refractive index on the wavelength and calculations of the efficiency coefficients SHG at a wavelength of 1064 nm were also carried out.

The dispersion of the refractive indices n_o and n_e is calculated in the range of 400−1200 nm. It is shown that the dependence $n(\lambda)$ is quite strong at relatively short wavelengths and it is practically absent at long wavelengths. In particular, at a wavelength of 532 nm, the double refraction in SNOH and BNOH will be equal to 0.174 and 0.063. The double refraction of Δn at a wavelength of 1064 nm is 0.148 and 0.063, respectively. For BNOH, there is a low dispersion of refractive indices, which is required from NLO materials. For a wavelength of 1064 nm, the SHG coefficients in KDP units are 1.61 in SNOH and 1.57 in BNOH. Thus, high values of SHG in strontium and barium nitrate hydrates do not follow from the calculated data.

11. Conclusion

Calculations of the crystal structure and physical properties of strontium and barium nitrate hydrates have been performed in the framework of the density functional theory with PBE, PBE0, and B3LYP functionals in the LCAO basis. Satisfactory agreement with the available crystallographic and optical data has been obtained.

The layered structure causes the anisotropy of bonding forces in crystals, which leads to specific features of elastic, dielectric, piezoelectric, and photoelastic properties. The volume compression modulus is two or more times greater than the shear modulus, which makes the crystals plastic. The different nature of atomic vibrations in the plane of the layer and between layers leads to LO-TO phonon shifts and provides a greater ionic than electronic contribution to the dielectric constant and piezoelectric constants. Calculations of the components of the polarizability, hyperpolarizability, and second-order electrical susceptibility tensors make it possible to calculate the second harmonic generation coefficients, which satisfactorily correlate with experimental ones at a wavelength of 106 nm.

The established correlations between the structure and the electronic, vibrational, mechanical, piezoelectric, and nonlinear optical properties of the studied hydrates of strontium and barium nitrates can be used to predict new NLO materials.

Conflict of interest

The authors declare that they have no conflict of interest.

References

[1] C. Wu, G. Yang, M.G. Humphrey, C. Zhang. Coord. Chem. Rev. **375**, 459 (2018).
[2] X. Liu, P. Gong, Y. Yang, G. Song, Z. Lin. Coord. Chem. Rev. **400**, 213045 (2019).
[3] Y. Liu, Y. Shen, S. Zhao, J. Luo. Coord. Chem. Rev. **407**, 213152 (2020).
[4] R.A. Kumar. Journal of Chemistry **2013**, 154862 (2013).
[5] D.A. Roberts. IEEEJ. Quantum Electron. **28**, 2057 (1992).
[6] L. Kang, Z. Lin. Light: Science & Applications. **11**, 201 (2022).
[7] B.I. Kidyarov. Crystals. **7**, 109 (2017).
[8] W. Wang, D. Mei, S. Wen, J. Wang, Y. Wu. J. Chinese Chemical Letters, **33**, *5*, 2301 (2022).
[9] P.S. Halasyamani, W. Zhang. Inorg. Chem. **56**, *20*, 12077 (2017).
[10] Y. Zhuravlev, V. Atuchin. Molecules **27**, *20*, 6840 (2022).
[11] S. Yun-Xia, L. Min, Y. Ning. Chinese J. Struct. Chem. **39**, *12*, 2148 (2020).
[12] L. Huang, G. Zou, H. Cai, S. Wang, C. Lin, N. Ye. J. Mater. Chem. C. **3**, 5268 (2015).
[13] X. Dong, L. Huang, Q. Liu, H. Zeng, Z. Lin, D. Xu, G. Zou. Chemical Communication **54**, *45*, 5792 (2018).
[14] S. Dill, K. Gibson, J. Glaser, S. Tragl, H.-J. Meyer. Z. Anorg. Allg. Chem. **633**, 274 (2007).
[15] L. Liu, Y. Yang, L. Li, Z. Yang, S. Pan. Journal of Alloys and Compounds **695**, 1719 (2017).
[16] B. Ribar, B. Matkovic, B. Prelesni, R. Herak, F. Gabela, Acta Crystallogr. A. **28**, 560 (1972).
[17] S. Kavitha, R.E. Vizhi. Journal of Molecular Structure **1276**, 134746 (2023).
[18] M.A. Khainovsky, E.V. Boldyreva, V.G. Tsirelson. Acta Cryst. B. **80**, 51 (2024).

[19] G. Clementi, F. Cottone, A. Di Michele, L. Gammaitoni, M. Mattarelli, G. Perna, M. López-Suárez, S. Baglio, C. Trigona, I. Neri. Energies **15**, 6227 (2022).
[20] A. Erba, R. Dovesi. Phys. Rev. B **88**, 045121 (2013).
[21] R.A. Evarestov, S.S. Novikov. FTT, **67**, *2*, 262 (2025). (in Russian).
[22] R. Dovesi, A. Erba, R. Orlando, C. M. Zicovich-Wilson, B. Civalleri, L. Maschio, M. Rérat, S. Casassa, J. Baima, S. Salustro, B. Kirtman. WIREs Comput Mol Sci. **8**, *4*, e1360 (2018).
[23] D.V. Oliveira, M.F. Peintinger, J. Laun, T. Bredow. J. Comput. Chem. **40**, 2364 (2019).
[24] J. Laun, D.V. Oliveira, T. Bredow. J. Comput. Chem. **39**, *19*, 1285 (2018).
[25] J. Laun, T. Bredow. J. Comput. Chem. **42**, *15*, 1064 (2021).
[26] J.P. Perdew, K. Burke, M. Ernzerhof. Phys. Rev. Lett. **77**, 3865 (1996).
[27] S. Grimme, S. Ehrlich, L. Goerigk. Comput. Chem. **32**, *7*, 1456 (2011).
[28] A.D. Becke. J. Chem. Phys. **98**, 5648 (1993).
[29] C. Lee, W. Yang, R.G. Parr. Phys. Rev. B **37**, 785 (1988).
[30] C. Adamo, V. Barone. J. Chem. Phys. **110**, 6158 (1999).
[31] R. Dovesi, V.R. Saunders, C. Roetti, R. Orlando, C.M. Zicovich-Wilson, F. Pascale, B. Civalleri, K. Doll, N.M. Harrison, I.J. Bush Ph. D'Arco, M. Llunel, M. Caus, Y. Noel, L. Maschio, A. Erba, M. Rerat, S. Casassal., CRYSTAL17 User's Manual, Universitá of Torin, Torino, Italy (2018).
[32] H.J. Monkhorst, J.D. Pack. Phys. Rev. B. **13**, 5188 (1976).
[33] F. Birch. Journal Geophysical Research **83**, *B3*, 1257 (1978).
[34] F. Pascale, C.M. Zicovich-Wilson, F.L. Gejo, B. Civalleri, R. Orlando, R. Dovesi. J. Comput. Chem. **25**, 888 (2004).
[35] C.M. Zicovich-Wilson, J. Torres, F. Pascale, L. Valenzano, R. Orlando, R. Dovesi. J. Comput. Chem. **29**, 2268 (2008).
[36] W.F. Perger, C. Criswell, B. Civalleri, R. Dovesi. Comp. Phys. Comm. **180**, *10*, 1753 (2009).
[37] A. Erba, A. Mahmoud, R. Orlando, R. Dovesi. Phys. Chem. Minerals **41**, 151 (2014).
[38] Yu.N. Zhuravlev, D.V. Korabelnikov. FTT **58**, *6*, 1129 (2016) (in Russian).
[39] Z. Hu, M. Lan, D. Huang, P. Huang, S. Wang. Crystals **12**, 1323 (2022).
[40] Yu.N. Zhuravlev, D.V. Korabelnikov. Izvestiya vysshikh uchebnykh zavedeniy. Fizika **60**, *1*, 123 (2017). (in Russian).
[41] H. Jia, F. Wang, J. Wu, X. Tan, Y. Cao. International Journal of Modern Physics B **34**, *30*, 2050286 (2020).
[42] M. Born, K. Huang. Dynamics Theory of Crystal Lattices. Oxford University Press, Oxford, UK (1954).
[43] F. Mouhat, F.-X. Coudert. Phys. Rev. B **90**, 224104 (2014).
[44] H.A. Abdullaev. FTT **48**, *4*, 623 (2006). (in Russian).
[45] Z. Sun, S. Li, R. Ahuja, J.M. Schneider. Solid State Commun. **129**, *9*, 589 (2004).
[46] W. Voigt. Lehrbuch der Kristallphysik. Teubner, Leipzig (1928). 978 p.
[47] A. Reuss. Z. Angew. Math. Mech. **9**, *1*, 4958 (1929).
[48] R. Hill. Journal of the Mechanics and Physics of Solids. **11**, *5*, 357 (1963).
[49] S.F. Pugh. Philos. Mag. J. Sci. **45**, 823 (1954).
[50] J. Haines, J.M. Léger, G. Bocquillon. Annual Review of Materials Research, **31**, 1 (2001).
[51] D.S. Sanditov, V.V. Mantov, B.D. Sanditov. ZhTF **79**, *4*, 150 (2009). (in Russian).
[52] J.P. Castagna, M.L. Batzle, R.L. Eastwood. Geophysics, **50**, 571 (1985).
[53] O.L. Anderson. J. Phys. Chem. Solids. **24**, 909 (1963).
[54] D.R. Clarke. Surf. Coat. Technol. **163**, 67 (2003).
[55] P. Huang, S. Wang, J. Ding, D. Wang, B. Wang, H. Liu, L. Xu, L. Zhang, X. Li, Y. Liu. RSC Adv. **9**, 20706 (2019).
[56] K.A. Hussain, P.M. Kumar, A. Saritha. Int. J. Innov. Res. Sci. Eng. Tech., **4**, 11146 (2015).
[57] R. Dovesi, M. De La Pierre, A.M. Ferrari, F. Pascale, L. Maschio, C.M. Zicovich-Wilson. Am. Miner. **96**, 1787 (2011).
[58] C. Carteret, M. De La Pierre, M. Dossot, F. Pascale, A. Erba, R. Dovesi. J. Chem. Phys. **138**, 014201 (2013).
[59] X. Gonze, C. Lee. Phys. Rev. B **55**, 10355 (1997).
[60] A. Erba, Kh.E. El-Kelany, M. Ferrero, I. Baraille, M. Rerat. Phys. Rev. B. **88**, 035102 (2013).
[61] J. Baima, A. Erba, L. Maschio, C.M. Zicovich-Wilson, R. Dovesi, B. Kirtman, Z. Phys. Chem. **230**, 719 (2016).
[62] A. Erba. Phys. Chem. Chem. Phys., **18**, 13984 (2016).
[63] R. Tarumi, K. Nakamura, H. Ogi, M. Hirao. Journal of Applied Physics. **102**, 113508 (2007).
[64] A.J. Lovinger. Ferroelectric Polymers. Science. **220**, 1115 (1983).
[65] A.V. Sotnikov, R. Kunze, H. Schmidt, M. Weihnacht, M. Hengst, J. Gotze. FTT **51**, *2*, 261 (2009) (in Russian).
[66] A. Erba, M.T. Ruggiero, T.M. Korter, R. Doves. J. Chem. Phys. **143**, 144504 (2015).
[67] L. Levien, C.T. Prewitt, D.J. Weidner. American Mineralogist. **65**, *9–10*, 920 (1980).
[68] A. Erba, M.T. Ruggiero, T.M. Korter, R. Dovesi. J. Chem. Phys. **143**, 144504 (2015).
[69] M. Ferrero, M. Rerat, R. Orlando, R. Dovesi. J. Chem. Phys. **128**, 014110 (2008).
[70] M. Ferrero, B. Civalleri, M. Rérat, R. Orlando, R. Dovesi. J. Chem. Phys. **131**, 214704 (2009).

Translated by A.Akhtyamov